The rotational excitation of the water isotopologues by molecular hydrogen

A Faure, M Zoltowski, L. Wiesenfeld, F Lique, A Bergeat

Monthly Notices of the ROYAL ASTRONOMICAL SOCIETY

MNRAS **527,** 3087–3093 (2024) https://doi.org/10.1093/mnras/stad3037
Advance Access publication 2023 October 05

The rotational excitation of the water isotopologues by molecular hydrogen

A. Faure [1]★ M. Żółtowski,[2,3] L. Wiesenfeld [4] F. Lique[3] and A. Bergeat[5]

[1] *Univ. Grenoble Alpes, CNRS, IPAG, F-38000 Grenoble, France.*
[2] *Univ. Le Havre Normandie, CNRS, LOMC, F-76600 Le Havre, France*
[3] *Univ. Rennes, CNRS, IPR (Institut de Physique de Rennes), F-35000 Rennes, France.*
[4] *Univ. Paris-Saclay, CNRS, Laboratoire Aimé Cotton, F-91405 Orsay, France*
[5] *Univ. Bordeaux, CNRS, ISM, F-33400 Talence, France*

Accepted 2023 October 3. in original form 2023 September 22

ABSTRACT

We present cross-sections and rate coefficients for rotational transitions in the water isotopologues D_2O, $H_2^{18}O$, and HDO induced by collisions with para-$H_2(j_2 = 0)$ and ortho-$H_2(j_2 = 1)$. Quantum scattering calculations are performed at the full close-coupling level with the isotopic variants of an accurate full-dimensional H_2O-H_2 interaction potential. The D_2O, $H_2^{18}O$, and HDO cross-sections are compared to the corresponding cross-sections for H_2O. Large isotopic effects are observed in the case of D_2O and HDO, in particular for collisions with p-$H_2(j_2 = 0)$, while the ^{18}O isotopic substitution is found to be negligible. Rate coefficients are provided for rotational transitions among all para-D_2O, ortho-D_2O, and HDO levels with internal energy below 300 cm^{-1} and for kinetic temperatures in the range 5–300 K. Non-LTE radiative transfer calculations show that the HDO 225.9 GHz and $H_2^{18}O$ 203.4 GHz transitions recently detected with ALMA in the young proto-planetary disc V883 Ori should be inverted (weak masers) in a large fraction of the disc.

Key words: astrochemistry – line: formation – masers – molecular data – molecular processes – scattering – .

1 INTRODUCTION

Isotopologues are molecules that differ only in their isotopic composition. In the case of water, the main isotopologue is $H_2^{16}O$ (hereafter denoted as H_2O). Stable rare isotopologues include the water-hydrogen isotopologues $HD^{16}O$ (denoted as HDO) and $D_2^{16}O$ (denoted as D_2O), the water-oxygen isotopologues $H_2^{17}O$ and $H_2^{18}O$, and the multiply substituted isotopologues $HD^{17}O$, $HD^{18}O$, $D_2^{17}O$, and $D_2^{18}O$. Among these nine stable isotopologues, H_2O, HDO, D_2O, $H_2^{17}O$, and $H_2^{18}O$ were all identified in the interstellar medium (ISM) (see van Dishoeck et al. 2021, and references therein). Very recently, HDO and $H_2^{18}O$ have been also detected in a young proto-planetary disc (Tobin et al. 2023).

Rare isotopologues are important for several reasons: first, from the observational point of view, the transitions of the main isotopologue of abundant molecules are often optically thick, which leads to difficulties both in deriving the column densities and in observing the inner part of astronomical sources. Secondly, the measurement of isotopic abundance ratios is a precious tool for the understanding of stellar nucleosynthesis, galactic chemical evolution, and isotopic fractionation processes. Third, the isotopic composition in the ISM, in protostars, and in proto-planetary discs can help to trace a possible interstellar heritage in Solar system materials, especially in comets. Of particular importance in this context are the D/H isotopic ratios which can help to evaluate e.g. the amount of water delivered by asteroids and comets to the Earth's oceans (where D/H $\sim 10^{-4}$). Orders of magnitude enrichments (with respect to the D/H solar value of 1.9×10^{-5}) in deuterated molecules are indeed observed in the ISM, in discs and in Solar system bodies (see Nomura et al. 2023; Tobin et al. 2023, and references therein). Oxygen isotopic fractionation is also observed in these sources, but with smaller variations with respect to the solar values $^{16}O/^{18}O \sim 530$ and $^{16}O/^{17}O \sim 2800$. Finally, the increased sensitivity of radio and millimetre telescopes allows the detection of an ever growing number of isotopologues in the ISM, including multiply substituted species.

Water isotopologues can be observed in the (sub)millimetre and infrared ranges, through rotational and ro-vibrational emission/absorption lines. The translation of observed spectra to accurate column densities and isotopic ratios requires however access to both spectroscopic and collisional data. Indeed, water molecules in the ISM are generally not at local thermodynamical equilibrium (LTE) because of the low density of the interstellar gas, which is mainly composed by molecular hydrogen (H_2). As a result, the relative occupation of the water energy levels cannot be described by a single 'excitation temperature'[1] and the radiative transfer must be solved simultaneously with the statistical equilibrium equations. An accurate knowledge of rate coefficients for inelastic collisions between water isotopologues and molecular hydrogen is thus necessary.

An extensive set of rate coefficients for the rotational (de)excitation of H_2O by H_2 in the kinetic temperature range 5–1500 K have been published by Daniel, Dubernet & Grosjean (2011). These include

★ E-mail: alexandre.faure@univ-grenoble-alpes.fr

[1]The excitation temperature of a transition is defined from the population ratio of the upper and lower levels using the Boltzmann equation.

the lowest 45 levels of both para- and ortho-H_2O (hereafter denoted as p-H_2O and o-H_2O) with angular momenta $j_1 \leq 11$ and two levels for both para-H_2 and ortho-H_2 with angular momenta $j_2 = 0$, 2 and $j_2 = 1$, 3, respectively. Quantum calculations including the coupling between rotation and bending of H_2O have been also obtained recently (Stoecklin et al. 2019; Wiesenfeld 2021, 2022), but for limited sets of transitions and kinetic temperatures. For HDO and D_2O, Faure et al. (2012) have published rotational rate coefficients for kinetic temperatures in the range 5–300 and 5–100 K, respectively. These include the lowest 30 levels of HDO for collisions with p-$H_2(j_2 = 0)$ and o-$H_2(j_2 = 1)$ and the six lowest levels of both p-D_2O and o-D_2O for collisions with p-$H_2(j_2 = 0)$. In all the above studies, the full nine-dimensional potential energy surface (PES) computed by Valiron et al. (2008) (hereafter denoted as V08) was employed. Finally, to the best of our knowledge, no collisional data exist for $H_2^{17}O$ and $H_2^{18}O$.

In this paper, we present extended and improved sets of rate coefficients for the rotational (de)excitation of HDO and D_2O by p-$H_2(j_2 = 0)$ and o-$H_2(j_2 = 1)$ (hereafter denoted as p-H_2 and o-H_2, respectively) in the kinetic temperature range 5–300 K. In addition, oxygen isotopic effects are investigated for the first time by computing cross-sections for the rotational excitation of $H_2^{18}O$ by H_2. In Section 2, we briefly introduce the PES for the three isotopic variants of H_2O-H_2 interaction. In Section 3, the quantum scattering calculations are described, and Section 4 presents cross-sections and rate coefficients for the three rare isotopologues. In Section 5, radiative transfer calculations are performed to illustrate non-LTE effects, including weak maser action, in the 225.9 and 241.6 GHz lines of HDO and the 203.4 GHz line of $H_2^{18}O$. A conclusion is given in Section 5.

2 POTENTIAL ENERGY SURFACES

The V08 full nine-dimensional H_2O-H_2 PES of Valiron et al. (2008) was employed in all scattering calculations presented next. This PES was computed at the CCSD(T) level of theory and it was then calibrated by higher accuracy explicitly correlated CCSD(T)-R12 calculations. It has been checked against various experimental data including elastic integral cross-sections, state-to-state inelastic differential cross-sections, pressure broadening cross-sections, and infrared spectra of the complex (see Drouin & Wiesenfeld 2012; Ziemkiewicz et al. 2012, and references therein). These comparisons have all confirmed the high quality of the PES. In addition, a recent experimental crossed-beam study was able to observe near-threshold resonances in rotational excitation cross-sections of H_2O and D_2O colliding with H_2 (Bergeat et al. 2020a, b, 2022). The excellent agreement with theory has certainly provided the most decisive test of the V08 PES. We note that two other full-dimensional PES for H_2O-H_2 have been published since 2008 (Homayoon et al. 2015; Li et al. 2022). Both were obtained at the explicitly correlated CCSD(T)-F12a level of theory and they should be of similar accuracy than the V08 PES. In particular, the three global minima are in good agreement, at ~ -240 cm^{-1} within a few cm^{-1}. We note that the CCSD(T)-F12a calculations of Li et al. (2022) were combined with MRCI-F12 calculations to provide, for the first time, a proper description of the hydrogen exchange and dissociation channels.

The collisional excitation of a rare isotopologue takes place on the same full-dimensional Born–Oppenheimer PES as the main isotopologue. Excitation differences between isotopologues therefore reflect the dynamical (nuclear) effects. Within the rigid-rotor approximation, these involve small changes in (i) the centre-of-mass position, (ii) the rotation of the principal axes of inertia (when the symmetry of the main isotopologue is broken), (iii) the state-averaged geometry (zero-point vibrational effects), (iv) the reduced mass of the total system, and (v) the energy level spacings. In practice, the rigid-rotor PES for HDO$-H_2$, D_2O-H_2, and $H_2^{18}O-H_2$ were obtained from the full flexible V08 H_2O-H_2 PES, but in the principal inertia axes of the specific rare isotopologue. In addition, the internal geometries (distances and angles) of HDO and D_2O were fixed at their ground-state vibrationally averaged values using the procedure explained in Scribano, Faure & Wiesenfeld (2010). This was unnecessary for $H_2^{18}O$ since the ^{18}O substitution changes the $-$OH distance by less than 1 per cent.

The general transformation from the isotopologue body-fixed frame to the original H_2O body-fixed frame (where the full-dimensional H_2O-H_2 PES is expressed) can be found in Wiesenfeld, Scribano & Faure (2011). As noted in Bergeat et al. (2020b), we found a small error in the numerical implementation of this transformation and the V08 PES routine was used to generate new corrected PESs for HDO$-H_2$ and D_2O-H_2 and the first PES for $H_2^{18}O-H_2$. The general coordinate system can be found in fig. 1 of Wiesenfeld et al. (2011). The water molecule lies in the xz plane. The ^{18}O substitution maintains the C_2 symmetry z-axis but shifts the centre of mass by $\delta z = 0.0127\ a_0$ towards the ^{18}O atom. Similarly, double deuteration of H_2O shifts the centre of mass by $\delta z = -0.0993\ a_0$ away from the ^{16}O atom. Finally, the single deuteration of H_2O causes both a shift of the centre of mass by $\delta x = 0.0761\ a_0$ and $\delta z = -0.0522\ a_0$ and a rotation of the inertia axes by an angle $\gamma = -21.04$ deg from the HDO to the H_2O body-fixed frame. The interaction energies for the HDO$-H_2$, D_2O-H_2, and $H_2^{18}O-H_2$ complexes were obtained following the procedure of Wiesenfeld et al. (2011), according to their Eqs. (3–6).[2] Grid points describing the angular coordinates of H_2 relative to the HDO, D_2O, and $H_2^{18}O$ body-fixed frames were chosen via random sampling for 28 fixed intermolecular distances in the range 3–14 a_0. Then, at each intermolecular distance, the interaction potential was least-squared fitted using the functional form employed by Valiron et al. (2008), where full details about the fitting procedure can be found. The final expansions include 149 angular functions for $H_2^{18}O-H_2$ and D_2O-H_2 (the same functions as for H_2O-H_2), and 175 angular functions for HDO$-H_2$.

3 SCATTERING CALCULATIONS

Scattering calculations were performed at the quantum close-coupling level by combining the MOLSCAT code (Hutson & Green 2012) with the three isotopic variants of the H_2O-H_2 PES described above. The isotopologues HDO, D_2O, and $H_2^{18}O$ are asymmetric tops with rotational constants taken as (in cm^{-1}) $A = 23.4140$, $B = 9.10340$, $C = 6.40628$ for HDO, $A = 15.4200$, $B = 7.27299$, $C = 4.84529$ for D_2O, and $A = 27.5313$, $B = 14.5218$, $C = 9.23809$ for $H_2^{18}O$. These values come from the JPL catalogue[3] (Pickett et al. 1998) for HDO and $H_2^{18}O$ and from the Cologne Database for Molecular Spectroscopy[4] (Müller et al. 2005) for D_2O. Centrifugal correction terms were found to be unnecessary to reproduce experimental level energies up to 300 cm^{-1} to within 1 cm^{-1}, which is appropriate at the investigated collisional energies

[2]Equation (5) in Wiesenfeld et al. (2011) should read $\tilde{\theta} = \arctan\sqrt{x_p^2 + y_p^2}/z_p$.

[3]https://spec.jpl.nasa.gov/

[4]https://cdms.astro.uni-koeln.de/

(see below).[5] The rotational energy levels of the water isotopologues are labelled by three quantum numbers: the angular momentum j_1 and the pseudo-quantum numbers k_a and k_c, which correspond to the projection of $\mathbf{j_1}$ along the principal inertia a and c axes. Owing to the non-zero nuclear spins of the H ($I = 1/2$) and D atoms ($I = 1$), D_2O and $H_2^{18}O$ present two spin modifications: para and ortho. The para-form corresponds to $k_a + k_c$ odd (even) for D_2O ($H_2^{18}O$) and the ortho-form corresponds to $k_a + k_c$ even (odd). Since the ortho and para levels do not interconvert in inelastic collisions, they were treated separately with MOLSCAT. For HDO, ortho/para modifications do not apply and all HDO levels are collisionally connected. For H_2, the rotational constant is taken as $B_0 = 59.322$ cm^{-1}, and the angular momentum is denoted as j_2. The collisional reduced mass (in amu) is 1.82252 for HDO−H_2, 1.83130 for D_2O−H_2, and 1.83123 for $H_2^{18}O$−H_2.

The coupled differential scattering equations were solved using the log-derivative (for HDO) and hybrid modified log-derivative Airy (for D_2O and $H_2^{18}O$) propagators (Alexander & Manolopoulos 1987) with a step size kept lower than 0.1 a_0. Other propagation parameters were taken as the MOLSCAT default values. Cross-sections were calculated for total energies up to 2000 cm^{-1} for HDO−H_2 and D_2O−H_2, and up to 300 cm^{-1} for $H_2^{18}O$−H_2. For this latter system, only test calculations were performed, as shown below. The energy step was varied between 0.25 cm^{-1} at low total energies (in order to account for the numerous resonances) and 100 cm^{-1} at the highest total energies (above 1000 cm^{-1}). The HDO and D_2O basis sets incorporated angular momenta up to $j_1 = 10$ to ensure that inelastic cross-sections for all transitions among levels below 300 cm^{-1} are converged to within ∼10 per cent. For $H_2^{18}O$, the basis set was restricted to $j_1 \leq 5$ because only low-lying levels were investigated. The inclusion of the $j_2 = 2$ level in the p-H_2 basis set was necessary. In contrast, the level $j_2 = 3$ in the o-H_2 basis set was found to have a negligible influence, except for a detailed description of resonances (Bergeat et al. 2022). It should be noted that the largest CPU effort was required for HDO because it has no ortho/para modifications and the number of coupled-channels at high total energy becomes exceedingly large, i.e. larger than 10 000. In order to limit the computational cost and memory requirements, the additional MOLSCAT parameter EMAX (used to limit basis functions to HDO plus H_2 energies less than EMAX) was set to 1000 cm^{-1} for p-H_2 and 1120 cm^{-1} for o-H_2. We note that Faure et al. (2012) resorted to the coupled-state approximation at the highest collisional energies.

Finally, for HDO and D_2O, rate coefficients $k(T)$ in the temperature range $T = 5$–300 K were calculated for each collisional transition ($j_{k_a k_c} \rightarrow j'_{k'_a k'_c}$) by integrating the cross-sections (σ) over a Maxwell–Boltzmann distribution of collision energies (E_{col}):

$$k(T_{\rm kin}) = \sqrt{\frac{8k_{\rm B}T_{\rm kin}}{\pi\mu}} \int_0^\infty \sigma(x) x \exp(-x) {\rm d}x, \quad (1)$$

where $x = E_{\rm col}/(k_{\rm B}T_{\rm kin})$, $k_{\rm B}$ is the Boltzmann constant, and μ is the collisional reduced mass.

[5]Note that for HDO, the theoretical rigid-rotor levels 4_{22} and 5_{05} are reversed with respect to the experimental order. However, because these levels are separated by only 0.11 cm^{-1}, the impact on cross-sections is entirely negligible, except at collisional energies lower than ∼1 cm^{-1}.

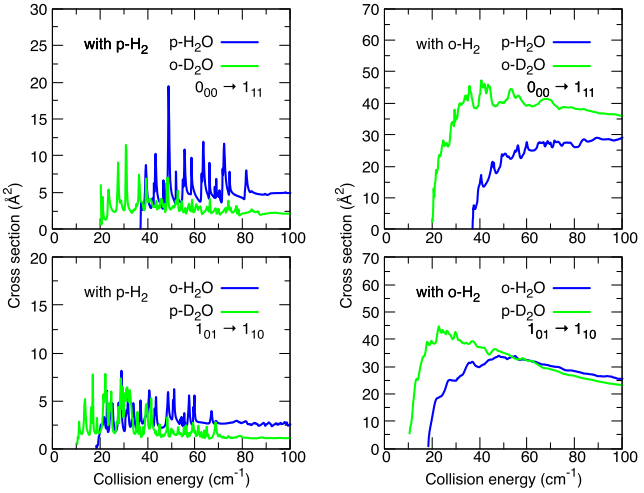

Figure 1. Comparison between H_2O and D_2O excitation cross-sections $0_{00} \rightarrow 1_{11}$ (upper panels) and $1_{01} \rightarrow 1_{10}$ (lower panels) as a function of the collision energy. Colliders p-H_2($j_2 = 0$) (left panels) and o-H_2($j_2 = 1$) (right panels) are considered.

4 CROSS-SECTIONS AND RATE COEFFICIENTS

A comparison between cross-sections for the dipole-allowed rotational transitions $0_{00} \rightarrow 1_{11}$ and $1_{01} \rightarrow 1_{10}$ in H_2O and D_2O is presented in Fig. 1. Cross-sections for H_2O were taken from the calculations presented in Bergeat et al. (2020a). We can first notice that the magnitude of the respective H_2O and D_2O cross-sections can differ by up to a factor of 2 (with p-H_2) and that these differences vary with both the transition and the collision energy. We also observe the presence of many scattering resonances, which occur when the collision energy matches the energy of a metastable bound-state of the collision complex. Such resonances have been observed experimentally in the D_2O transitions $1_{01} \rightarrow 1_{10}$ and $0_{00} \rightarrow 1_{11}$ for collisions with 'normal'-H_2 (3:1 ortho:para mixture) (Bergeat et al. 2022) and, more spectacularly, in the transition $0_{00} \rightarrow 2_{02}$ for collisions with p-H_2 (Bergeat et al. 2020b). The resonance pattern is indeed much larger for p-H_2 than for o-H_2 simply because o-H_2 resonances are hidden under a larger background (see Fig. 1). This can be explained by the non-vanishing quadrupole of o-H_2 and the stronger binding with o-H_2($j_2 = 1$) than with p-H_2($j_2 = 0$) (the H_2 quadrupole in the state $j_2 = 0$ is zero by symmetry), which significantly increases the potential well, the PES anisotropy, and the number of bound-states in the complex. As a result, the cross-sections for o-H_2 exceed those for p-H_2 by a factor of ∼5–10. It should be noted, however, that much smaller differences between o-H_2 and p-H_2 are observed in the case of dipole-forbidden transitions (e.g. those with $\Delta j_1 = 2$), as shown in the rate coefficients below. Finally, the change in rotational thresholds (lowered by ∼10–20 cm^{-1} for D_2O) are also clearly visible, which will affect the excitation rate coefficients at low kinetic temperature. For a more complete discussion about resonance and near-threshold effects, the reader is referred to Bergeat et al. (2020b) and Bergeat et al. (2022).

Cross-sections for the same transitions in $H_2^{18}O$ are displayed in Fig. 2. In this case, differences with H_2O are hardly visible and amount to no more than 10 per cent, which is similar to our convergence criterion. Resonance peaks are also only slightly shifted downwards, by less than 0.25 cm^{-1}. This demonstrates that the ^{18}O isotopic substitution is negligible at our level of accuracy and that the H_2O inelastic cross-sections can be employed for $H_2^{18}O$ and even

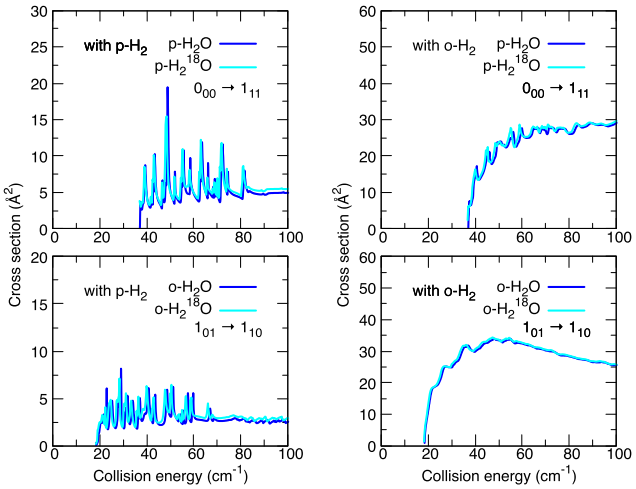

Figure 2. Comparison between H_2O and $H_2^{18}O$ excitation cross-sections $0_{00} \rightarrow 1_{11}$ (upper panels) and $1_{01} \rightarrow 1_{10}$ (lower panels) as a function of the collision energy. Colliders p-H_2($j_2 = 0$) (left panels) and o-H_2($j_2 = 1$) (right panels) are considered.

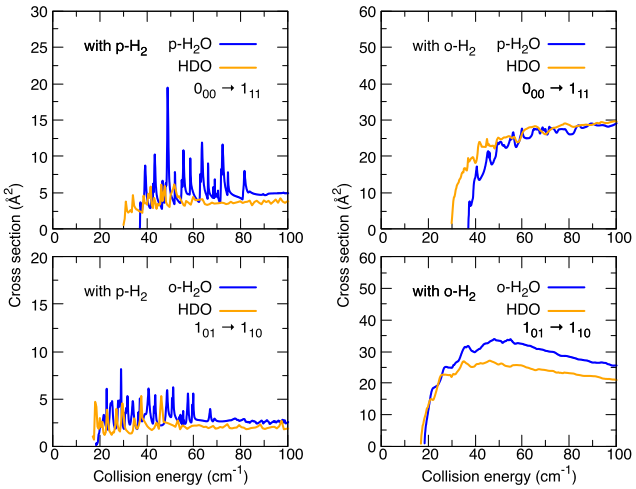

Figure 3. Comparison between H_2O and HDO excitation cross-sections $0_{00} \rightarrow 1_{11}$ (upper panels) and $1_{01} \rightarrow 1_{10}$ (lower panels) as a function of the collision energy. Colliders p-H_2($j_2 = 0$) (left panels) and o-H_2($j_2 = 1$) (right panels) are considered.

more so for $H_2^{17}O$ where the isotopic shift of the centre of mass is even smaller ($\delta z = 0.00670\ a_0$ towards the ^{17}O atom versus $\delta z = 0.0127\ a_0$ towards the ^{18}O atom).

The same dipole-allowed transitions in HDO are shown in Fig. 3. It is useful to recall that the single deuterium substitution causes both a shift of the centre of mass and a rotation of the inertia axes. This latter rotation makes the HDO dipole to have components along the two in-plane axes of inertia so that in addition to *b*-type radiative transitions (odd Δk_a and odd Δk_c), *a*-type radiative transitions (even Δk_a and odd Δk_c) are dipole-allowed in HDO. Collisionally, all HDO levels being connected (no ortho/para modification), many more collisional transitions are allowed in HDO than in H_2O or D_2O, as shown in the rate coefficients below. In Fig. 3, the magnitude of the respective H_2O and HDO background cross-sections are found to differ by less than 20 per cent for the plotted transitions (but larger differences are observed for other transitions). On the other hand, the resonance pattern with p-H_2 is stronger and more pronounced in H_2O than

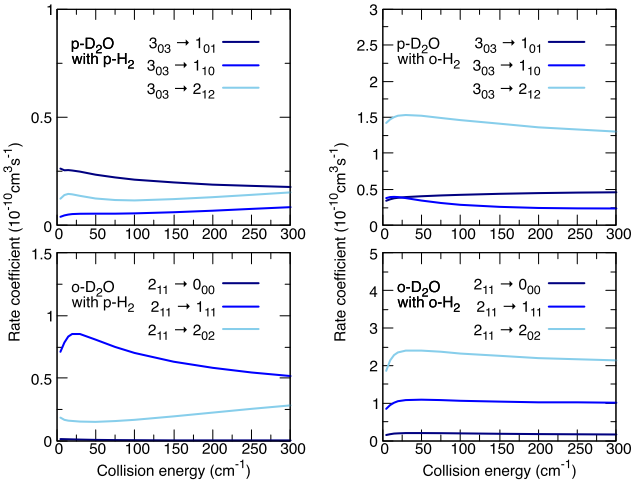

Figure 4. Rate coefficients as a function of temperature for de-excitation of the 3_{03} (upper levels) and 2_{11} (lower levels) levels of p-D_2O and o-H_2O, respectively, in collisions with p-H_2 (left panels) and o-H_2 (right panels).

in HDO, due to less closed-channels and overlapping resonances. Finally, cross-sections with o-H_2 are again found to be much larger than those for p-H_2

Rate coefficients for D_2O are displayed in Fig. 4, where the initial level 3_{03} (2_{11}) is the fourth-lowest level in energy of p-D_2O (o-D_2O) and the final levels are the three lower available levels. We can first observe that the rate coefficients display non-monotonic temperature dependences. The rate coefficients for o-H_2 are also found to be much larger than those for p-H_2, by up to a factor of 10 for the radiatively dipole-allowed transitions ($3_{03} \rightarrow 2_{12}$ and $2_{11} \rightarrow 2_{02}$), as expected. Much smaller differences are found for the dipole-forbidden transitions. It is also interesting to notice that the relative order of the rate coefficients significantly differs between p-H_2 and o-H_2: the radiatively dipole-forbidden transitions ($3_{03} \rightarrow 1_{01}$ and $2_{11} \rightarrow 1_{11}$) are favoured with p-$H_2$, while the radiatively dipole-allowed transitions ($3_{03} \rightarrow 2_{12}$ and $2_{11} \rightarrow 2_{02}$) dominate with o-$H_2$. As explained above, this is due to the non-vanishing dipole–quadrupole interaction for collisions with H_2 when $j_2 > 0$.

The above comments generally apply also to the main isotopologue H_2O, as shown in Fig. 5 where we report the rate coefficients computed by Daniel et al. (2011), as provided in the BASECOL data base (Dubernet et al. 2013). We note, however, significant differences between H_2O and D_2O for individual state-to-state transitions, especially for collisions with p-H_2 where the H_2O and D_2O respective individual rate coefficients can differ by up to a factor of 4. On the other hand, for collisions with o-H_2, the H_2O and D_2O rate coefficients agree to within 50 per cent. Again, this difference between p-H_2 and o-H_2 can be attributed to the long-range quadrupolar interaction terms (e.g. dipole–quadrupole) of the PES, which are much less sensitive to the H/D substitution than the weaker and more anisotropic short-range terms. Both kinematic (mass and velocities) and PES effects thus play a role in the observed isotopic effects.

Rate coefficients for HDO are displayed in Fig. 6, where the initial level 2_{11} is the seventh-lowest level in energy and the final levels are the six lower available levels. Transitions forbidden (by symmetry) in H_2O and D_2O are plotted in the upper panels, while the lower panels show the transitions reported in the lower panels of Figs 4 and 5. Radiatively, the dipole-allowed transitions are $2_{11} \rightarrow 1_{10}$ ($A = 1.65 \times 10^{-3}$ s^{-1}), $2_{11} \rightarrow 2_{02}$ ($A = 3.46 \times 10^{-3}$ s^{-1}), and $2_{11} \rightarrow$

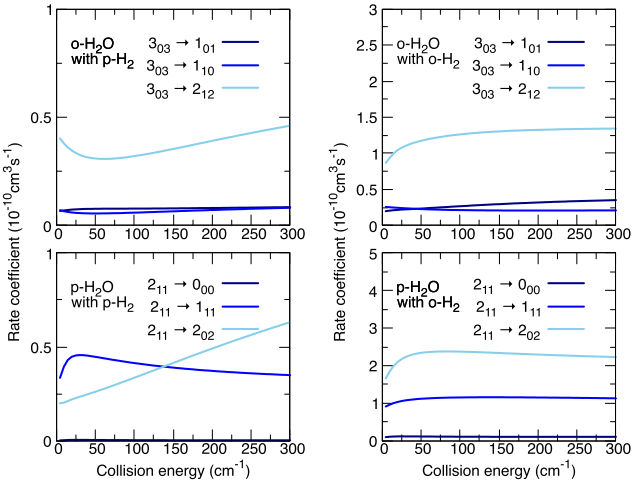

Figure 5. Rate coefficients as a function of temperature for de-excitation of the 3_{03} (upper panels) and 2_{11} (lower panels) levels of o-H_2O and p-H_2O, respectively, in collisions with p-H_2 (left panels) and o-H_2 (right panels). Data are taken from Daniel et al. (2011).

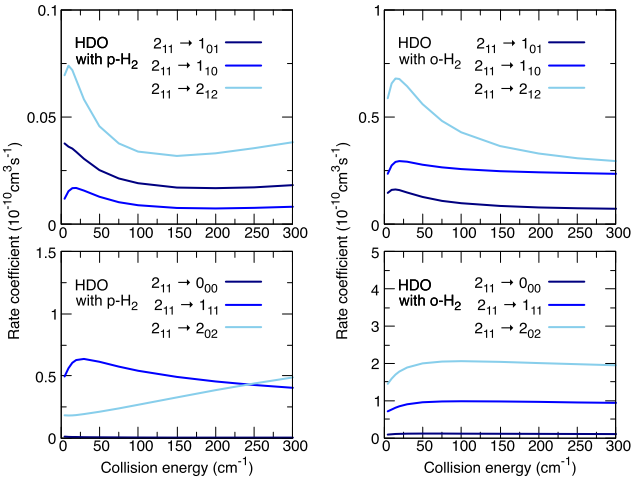

Figure 6. Rate coefficients as a function of temperature for de-excitation of the 2_{11} level of HDO in collisions with p-H_2 (left panels) and o-H_2 (right panels). Transitions forbidden in H_2O and D_2O are displayed in the upper panels.

2_{12} ($A = 1.19 \times 10^{-5}$ s^{-1}), where Einstein coefficients are taken from the JPL catalogue. Collisionally, the favoured transition with p-H_2 is $2_{11} \rightarrow 1_{11}$ (except above 250 K), while transition $2_{11} \rightarrow 2_{02}$ dominates for collisions with o-H_2. This, once again, reflects the role of the dipole–quadrupole interaction for collisions with o-H_2. More generally, we observe that the transitions forbidden in D_2O and H_2O have significantly smaller rate coefficients than those allowed in the C_2-symmetric isotopologues. This can be explained by the relatively small rotation of the inertia axes in HDO, which in particular maintains the strongest dipole component along the *b*-axis (1.732 D against 0.657 D along the *a*-axis). If we now compare HDO to D_2O for collisions with p-H_2, we can observe very similar magnitudes and temperature dependences of the respective individual rate coefficients. For collisions with o-H_2, as expected, the agreement between HDO, D_2O, and H_2O is generally good and within 50 per cent.

We note that the differences with the previous D_2O and HDO rate coefficients of Faure et al. (2012) were checked and found to be less than 20 per cent for collisions with o-H_2. For collisions with p-H_2, differences are generally within a factor of ∼2 and are mainly due to the implementation error in the frame transformation. As we will see next, the impact on radiative transfer calculations should be negligible at temperatures above 100 K where o-H_2 is the dominant collider.

Finally, it should be noted that at kinetic temperatures above ∼50 K or in the presence of radiative pumping, H_2 molecules in excited levels $j_2 = 2, 3$, etc. can contribute to the (de)excitation of molecules. It has been found, however, that the rate coefficients for collisions with $H_2(j_2 > 1)$ differ on average by less than ∼20 per cent from those for collisions with o-$H_2(j_2 = 1)$ (see Demes et al. 2023, and references therein). This result is robust for targets in their ground vibrational state and for rotational levels or kinetic temperatures below ∼500 K, so that near-resonance effects between the target and H_2 can be neglected. This means here that rate coefficients for collisions with $H_2(j_2 > 1)$ can be assumed equal to those for o-$H_2(j_2 = 1)$. In radiative transfer calculations, a simple recipe is to assign the present rate coefficients for collisions with o-$H_2(j_2 = 1)$ to the volume density of all H_2 levels with $j_2 \geq 1$. In general, H_2 levels can also be assumed thermalized, with a fixed or thermalized ortho-to-para ratio (OPR).

5 RADIATIVE TRANSFER CALCULATIONS

In order to estimate the impact of our new rate coefficients on the modelling of water isotopologue spectra, we have performed non-LTE radiative transfer calculations for HDO and p-$H_2^{18}O$, using for this latter the p-H_2O rate coefficients from Daniel et al. (2011). This choice was motivated by the recent ALMA observations of these two water isotopologues towards the young proto-planetary disc V883 Ori (Tobin et al. 2023). Three emission rotational lines have been detected: the $3_{12} \rightarrow 2_{21}$ and $2_{11} \rightarrow 2_{12}$ HDO lines at 225.9 GHz and 241.6 GHz, respectively, and the $3_{13} \rightarrow 2_{20}$ line of $H_2^{18}O$ at 203.4 GHz. Column densities were estimated by Tobin et al. (2023) assuming that the lines are optically thin and in LTE. These two assumptions are discussed below.

The RADEX program (van der Tak et al. 2007) was employed using the Large Velocity Gradient formalism for an expanding sphere. The rotational energy levels and radiative rates were taken from the JPL catalogue (Pickett et al. 1998). The HDO and p-$H_2^{18}O$ column densities were both fixed at 5×10^{15} cm^{-2}, which is close to the disc-averaged values determined by Tobin et al. (2023) (6.98×10^{15} and 5.52×10^{15} cm^{-2}, respectively), with an estimated line widh (full width at half-maximum) of 2 km s^{-1}. The hydrogen density was varied in the range 10^5–10^{10} cm^{-3}, which covers typical densities in the upper layers and mid-plane of V883 Ori. Three kinetic temperatures ($T_{\rm kin}$) were selected, 100, 200, and 300 K, which enclose the excitation temperatures derived by Tobin et al. (2023) (their fiducial model gives $T_{\rm kin} = 199 \pm 42$ K). No radiation field other than the cosmic microwave background at 2.73 K was considered. The OPR of $H_2^{18}O$ was fixed at 3. The H_2 levels with $j_2 > 1$ (of importance above 100 K) were included by assigning them the rate coefficients for o-$H_2(j_2 = 1)$, assuming thermal populations and a thermal OPR as recommended above. The previous set of rate coefficients computed by Faure et al. (2012) for HDO was also used at 200 K, in order to check the impact of the rate coefficient uncertainties.

In Fig. 7, we have plotted the excitation temperature ($T_{\rm ex}$) of the three detected lines as a function of the hydrogen density and for the three selected kinetic temperatures. At low hydrogen density,

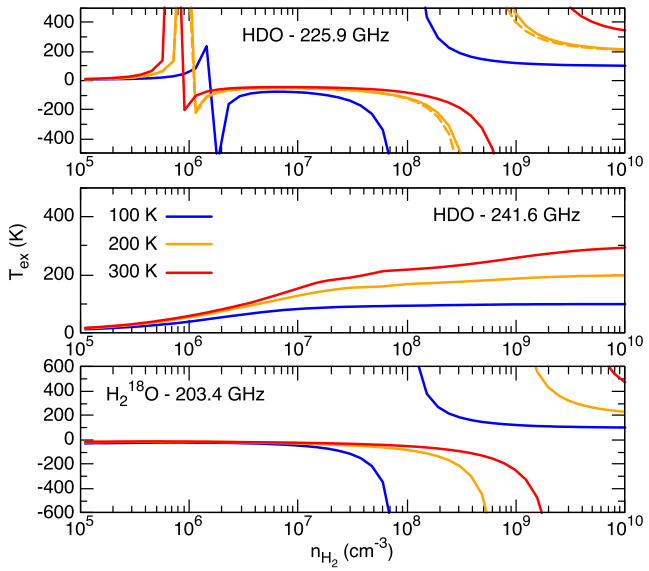

Figure 7. Excitation temperature of the three detected lines towards V883 Ori (the $3_{12} \rightarrow 2_{21}$ and $2_{11} \rightarrow 2_{12}$ HDO lines at 225.9 GHz and 241.6 GHz, respectively, and the $3_{13} \rightarrow 2_{20}$ line of $H_2^{18}O$ at 203.4 GHz) as a function of hydrogen density. The three selected temperatures are denoted in blue (100 K), orange (200 K), and red (300 K). The dashed orange line (panel of HDO at 225.9 GHz) corresponds to RADEX calculations at 200 K using the HDO collision data of Faure et al. (2012).

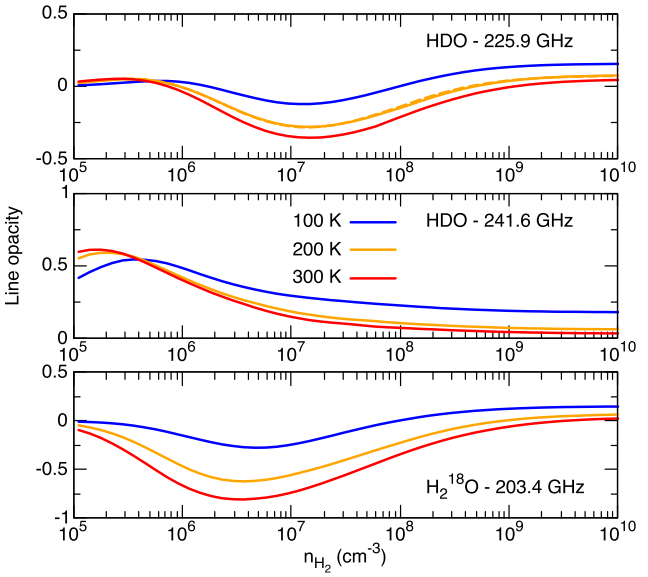

Figure 8. Line opacity of the three detected lines towards V883 Ori (the $3_{12} \rightarrow 2_{21}$ and $2_{11} \rightarrow 2_{12}$ HDO lines at 225.9 and 241.6 GHz, respectively, and the $3_{13} \rightarrow 2_{20}$ line of $H_2^{18}O$ at 203.4 GHz) as a function of hydrogen density. The three selected temperatures are denoted in blue (100 K), orange (200 K), and red (300 K). The dashed orange line (panel of HDO at 225.9 GHz) corresponds to RADEX calculations at 200 K using the HDO collision data of Faure et al. (2012).

the excitation temperatures of the two HDO lines are a few Kelvins above 2.73 K, suggesting populations close the radiative equilibrium. The T_{ex} then increase with density, as expected, but collisions are found to quickly invert the 225.9 GHz transition with the population inversion persisting up to densities $\sim 10^8$–10^9 cm^{-3}, depending on the kinetic temperature. It should be noted that this maser effect in dense and warm regions of proto-planetary discs was already predicted by Ceccarelli et al. (2010) (see also Faure et al. 2012 where six other HDO lines in the range 0–2000 GHz were found to invert at similar physical conditions). In contrast, the T_{ex} of the 241.6 GHz transition increases monotically and the LTE plateaus (where $T_{ex} = T_{kin}$) are reached above $\sim 10^8$–10^9 cm^{-3}. In the case of $H_2^{18}O$, we can observe that the 203.4 GHz transition is inverted over an even larger density range and up to $n_{H_2} \sim 3 \times 10^9$ cm^{-3} at $T_{kin} = 300$ K. We note that this line ($3_{13} \rightarrow 2_{20}$) is a well-known maser at 183.3 GHz in the main water isotopologue (see e.g. Neufeld et al. 2017, and references therein). The previous data set of Faure et al. (2012) (dashed orange line) provides very similar excitation temperatures for HDO, as expected.

Using the parametrized model of Tobin et al. (2023) for V883 Ori, we found that the density in the upper layers and mid-plane of the disc varies in the range $\sim 10^6$–10^{10} cm^{-3}. For instance, at a typical radius of 80 au the density is $\sim 6 \times 10^6$ cm^{-3} at a height of 50 au and $\sim 5 \times 10^9$ cm^{-3} at a height of 10 au. As a result, for the 225.9 and 203.4 GHz transitions, the LTE assumption does not apply in V883 Ori, except possibly for the emission from the most dense lower layers where the density exceeds $\sim 10^9$–10^{10} cm^{-3}. On the other hand, the HDO 241.6 GHz transition should thermalize as soon as the density reaches $\sim 10^8$ cm^{-3}.

The assumption of LTE by Tobin et al. (2023) relies on their estimates of the critical densities (n_{cr}) at 200 K for the detected transitions: they used the ratio of the spontaneous radiative rate to the collisional de-excitation rate, i.e. $n_{cr}(i \rightarrow f) = A(i \rightarrow f)/k(i \rightarrow f)$, and derived for the HDO 225.9, 241.6 and $H_2^{18}O$ 203.4 GHz transitions critical densities of 9.7×10^5, 1.1×10^6, and 3.8×10^5 cm^{-3}, respectively, which are not consistent with the above results. Indeed the conditions for LTE should be fulfilled for densities $n_{H_2} \gtrsim 100 n_{cr}$. In fact, for a polyatomic non-linear molecule, the critical density should be computed for an upper level i as the ratio between the sum of all possible spontaneous radiative rates to the sum of all possible collisional rate coefficients out of this level, i.e. $n_{cr}(i) = \sum_f A(i \rightarrow f)/\sum_f k(i \rightarrow f)$. This gives critical densities (at 200 K) of 9.3×10^7, 3.3×10^7 and 5.3×10^8 cm^{-3}, respectively, in good agreement with the LTE plateaus shown in Fig. 7.

Finally, the line opacity of the three detected lines, as computed by RADEX, are displayed in Fig. 8. With the chosen column densities of 5×10^{15} cm^{-2}, opacities (or their absolute values) are always lower than 1 but they can exceed $\sim$0.3 for densities below $\sim 10^8$ cm^{-3}, depending on the kinetic temperature. The assumption of optically thin lines is thus questionable.

In summary, the assumption that the three water lines detected in V883 Ori are optically thin and in LTE is not justified except in the most dense regions of the disc where the density exceeds $\sim 10^8$ cm^{-3}. Furthermore, two of the three transitions detected by Tobin et al. (2023) are potential weak masers, suggesting strong deviations from LTE in some regions of the disc. We note, however, that the contribution of the dust far-infrared radiation in pumping the HDO and $H_2^{18}O$ levels was neglected in our calculations. Ideally, a detailed non-LTE 2D radiative transfer model is required to properly fit the ALMA water spectra towards V883 Ori. Now it is not clear if the HDO/H_2O ratio derived by Tobin et al. (2023) will be substantially modified. As discussed by these authors, previous modelling studies of the same three transitions in protostars have shown that the HDO/H_2O ratios derived from non-LTE models differ from optically thin LTE calculations by a factor of 'only' 3–4 (see e.g. Persson et al. 2014). A robust determination of the HDO/H_2O would certainly require a careful non-LTE modelling, but

also the detection of additional water lines for better contraints on the excitation conditions. In any case, the uncertainties in the collisional rate coefficients have been removed in this study.

6 CONCLUSIONS

We have reported new cross-sections and rate coefficients for rotational transitions in D_2O, $H_2^{18}O$, and HDO induced by collisions with p-H_2($j_2 = 0$) and o-H_2($j_2 = 1$) in the kinetic temperature range 5–300 K. Scattering calculations were performed at the close-coupling level with the isotopic variants of the H_2O-H_2 PES of Valiron et al. (2008). By comparing the rotational cross-sections for transitions in D_2O, $H_2^{18}O$, and HDO to those in H_2O, we have shown that the deuterium isotopic substitution has a large impact, especially for collisions with p-H_2, where differences up to a factor of 4 were observed. Isotopic effects are caused by the (small) changes in the centre-of-mass position, internal geometry, reduced mass, and rotational constants. They thus reflect both kinematic (mass and velocities) and PES effects. In addition, the rotation of the principal inertia axes in HDO induces collisional transitions otherwise forbidden in the C_2-symmetric isotopologues. Rate coefficients for collisions with o-H_2($j_2 = 1$) were found to be larger than those for collisions with p-H_2($j_2 = 0$), in particular for dipole-allowed transitions due to the non-vanishing quadrupole of H_2($j_2 \geq 1$). In contrast, the ^{18}O isotopic substitution was found to be negligible so that the rate coefficients for H_2O can be reliably used for $H_2^{18}O$ and $H_2^{17}O$. Rate coefficients are provided for rotational transitions among all p-D_2O, o-D_2O, and HDO levels below 300 cm^{-1} and for kinetic temperatures in the range 5–300 K.

The relevance of the collisional rate coefficients was illustrated by performing RADEX calculations to mimic the excitation conditions in the V883 Ori proto-planetary disc where two HDO lines at 225.9 and 242.6 GHz and one $H_2^{18}O$ line at 203.4 GHz were recently detected with ALMA. Strong deviations from LTE, including population inversion in the lines at 225.9 and 203.4 GHz, were observed over a large range of densities and kinetic temperatures, suggesting that the assumption that the three lines are in LTE is not reliable in this source. Non-LTE (ideally 2D) radiative transfer models should be thus used for a robust determination of the HDO/H_2O ratio via the HDO and $H_2^{18}O$ column densities. Such models are still hampered by the small number of detected lines and by their dependence on the disc physical and chemical structure, but the collisional rate coefficients for the water isotopologues should no longer be considered as a limiting factor. In this context, we finally note that new crossed-beam experiments are in progress in Bordeaux to measure near-threshold cross-sections for HDO colliding with H_2.

ACKNOWLEDGEMENTS

This work was partly supported by the French Agence Nationale de la Recherche (ANR-Waterstars), contract ANR-20-CE31-0011. Part of the computations presented in this paper were performed using the GRICAD infrastructure (https://gricad.univ-grenoble-alpes.fr), which is supported by Grenoble research communities. The HDO computations were performed due to the IDRIS-CNRS contract A0120810769. We wish to acknowledge the support from the CEA/GENCI for awarding us access to the TGCC/IRENE supercomputer within the A0110413001 project. MZ wishes to acknowledge the support from the Wroclaw Centre of Networking and Supercomputing. FL acknowledges the Institut Universitaire de France.

DATA AVAILABILITY

The full set of spectroscopic and collisional data for HDO and D_2O will be made available through the EMAA data base (https://dx.doi.org/10.17178/EMAA) compiled by Alexandre Faure and Aurore Bacmann from IPAG, Grenoble. Other data are also available on reasonable request.

REFERENCES

Alexander M. H., Manolopoulos D. E., 1987, J. Chem. Phys., 86, 2044
Bergeat A., Faure A., Morales S. B., Moudens A., Naulin C., 2020a, J. Phys. Chem. A, 124, 259
Bergeat A., Morales S. B., Naulin C., Wiesenfeld L., Faure A., 2020b, Phys. Rev. Lett., 125, 143402
Bergeat A., Faure A., Wiesenfeld L., Miossec C., Morales S. B., Naulin C., 2022, Molecules, 27, 7535
Ceccarelli C., Cernicharo J., Ménard F., Pinte C., 2010, ApJ, 725, L135
Daniel F., Dubernet M. L., Grosjean A., 2011, A&A, 536, A76
Demes S., Lique F., Loreau J., Faure A., 2023, MNRAS, 524, 2368
Drouin B., Wiesenfeld L., 2012, Phys. Rev. A, 86, 022705
Dubernet M. L. et al., 2013, A&A, 553, A50
Faure A., Wiesenfeld L., Scribano Y., Ceccarelli C., 2012, MNRAS, 420, 699
Homayoon Z., Conte R., Qu C., Bowman J. M., 2015, J. Chem. Phys., 143, 084302
Hutson J. M., Green S., 2012, Astrophysics Source Code Library, record ascl: 1206.004
Li J., Liu Y., Guo H., Li J., 2022, Phys. Chem. Chem. Phys., 24, 27548
Müller H. S. P., Schlöder F., Stutzki J., Winnewisser G., 2005, J. Mol. Struct., 742, 215
Neufeld D. A. et al., 2017, ApJ, 843, 94
Nomura H. et al., 2023, in Inutsuka S., Aikawa Y., Muto T., Tomida K., Tamura M.eds, ASP Conf. Ser.Vol. 534, Protostars and Planets VII. Astron. Soc. Pac., San Francisco, p. 1075
Persson M. V., Jørgensen J. K., van Dishoeck E. F., Harsono D., 2014, A&A, 563, A74
Pickett H. M., Poynter R. L., Cohen E. A., Delitsky M. L., Pearson J. C., Müller H. S. P., 1998, J. Quant. Spec. Radiat. Transf., 60, 883
Scribano Y., Faure A., Wiesenfeld L., 2010, J. Chem. Phys., 133, 231105
Stoecklin T., Denis-Alpizar O., Clergerie A., Halvick P., Faure A., Scribano Y., 2019, J. Phys. Chem. A, 123, 5704
Tobin J. J. et al., 2023, Nature, 615, 227
Valiron P., Wernli M., Faure A., Wiesenfeld L., Rist C., Kedžuch S., Noga J., 2008, J. Chem. Phys., 129, 134306
van der Tak F. F. S., Black J. H., Schöier F. L., Jansen D. J., van Dishoeck E. F., 2007, A&A, 468, 627
van Dishoeck E. F. et al., 2021, A&A, 648, A24
Wiesenfeld L., 2021, J. Chem. Phys., 155, 071104
Wiesenfeld L., 2022, J. Chem. Phys., 157, 174304
Wiesenfeld L., Scribano Y., Faure A., 2011, Phys. Chem. Chem. Phys., 13, 8230
Ziemkiewicz M. P., Pluetzer C., Nesbitt D. J., Scribano Y., Faure A., van der Avoird A., 2012, J. Chem. Phys., 137, 084301

This paper has been typeset from a TEX/LATEX file prepared by the author.